Check for updates

View Article Online
View Journal

Nanoscale

Accepted Manuscript

This article can be cited before page numbers have been issued, to do this please use: H. Kim, M. Ko, S. Nam, S. Kim, Y. Jeong, S. M. Park, Y. R. Do and J. K. Song, *Nanoscale*, 2025, DOI: 10.1039/D5NR02469B.

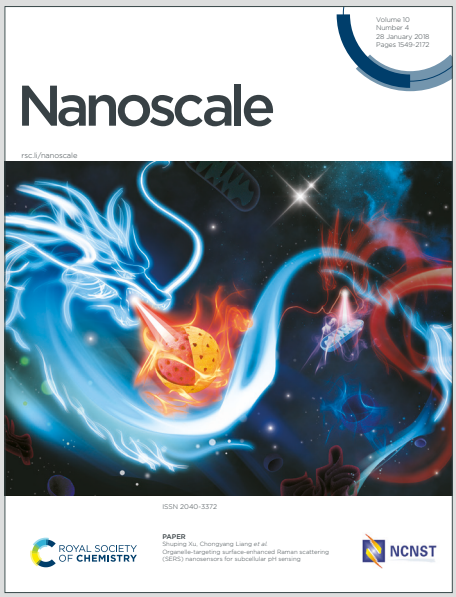

This is an Accepted Manuscript, which has been through the Royal Society of Chemistry peer review process and has been accepted for publication.

Accepted Manuscripts are published online shortly after acceptance, before technical editing, formatting and proof reading. Using this free service, authors can make their results available to the community, in citable form, before we publish the edited article. We will replace this Accepted Manuscript with the edited and formatted Advance Article as soon as it is available.

You can find more information about Accepted Manuscripts in the Information for Authors.

Please note that technical editing may introduce minor changes to the text and/or graphics, which may alter content. The journal's standard Terms & Conditions and the Ethical guidelines still apply. In no event shall the Royal Society of Chemistry be held responsible for any errors or omissions in this Accepted Manuscript or any consequences arising from the use of any information it contains.

ROYAL SOCIETY OF CHEMISTRY

rsc.li/nanoscale

Please do not adjust margins

ROYAL SOCIETY OF CHEMISTRY
View Article Online
DOI: 10.1039/D5NR02469B

Nanoscale

PAPER

Heterostructure Nanodisks for Multicolor Polariton Lasers with Controllable Whispering–Gallery Modes †

Received 00th January 20xx,
Accepted 00th January 20xx

DOI: 10.1039/x0xx00000x

www.rsc.org/

Haneul Kim,[‡a] Minji Ko,[‡b] Sangwon Nam,[a] Soyeon Kim,[b] Yujeong Jeong,[b] Seung Min Park,[a] Young Rag Do,*[b] and Jae Kyu Song*[a]

Highly efficient optoelectronic devices of ultrasmall sizes are demanded for building blocks of next-generation integrated circuits, where tunable color enhances the feasibility of various applications. Here, we realize tunable multicolor nanolasers using disk-shaped axial heterostructures composed of III-nitride materials (GaN/InGaN/GaN), leveraging the optical confinement effect and active waveguiding. In heterostructure nanodisks, the development of exciton–polariton induces unique features near the resonance regime and the formation of whispering–gallery modes facilitates optical gain processes for the polaritonic lasing of GaN. Likewise, the polaritonic lasing of InGaN emerges, although the small gain volume in the quantum well structure hinders the strong amplification. Notably, the characteristics of lasing differ between GaN and InGaN, suggesting a distinctive polariton behavior in quantum well structures. The alloyed systems enable tunable laser colors in the visible region, while whispering–gallery modes afford independent control of lasing. Therefore, we establish tunable dual-color polariton nanolasers using heterostructure disks for the first time, promising nanophotonic devices to take advantage of the optical confinement effect and active waveguiding.

1. Introduction

Ultraviolet light sources have been employed in a broad range of photonic and optoelectronic devices,[1-5] which are usually obtained from semiconductors with wide band gap structures.[6–10] Among them, GaN-based materials show high oscillator strengths and easy fabrication processes for versatile applications, including tunable light in the ultraviolet and visible regions for light-emitting diodes and laser diodes with the high quantum efficiency, long-term stability, and wide color gamut.[11-15] However, the realization of small devices still remains challenging, due to the difficulty in preparation of high-quality materials.[16,17] Besides, supplementary assemblies are typically required to increase efficiency, impeding the development of small devices.[18,19] Hence, the unique features of nanomaterials have attracted attention to realize small devices, because nanomaterials can serve as both the gain medium and optical cavity to achieve highly efficient nanolasers.[20-23]

The waveguiding properties of nanocavities, such as the rod, sphere, and disk, facilitate the optical gain process with reduced device complexity. Indeed, nanorod lasers have been extensively reported using Fabry–Pérot-type cavities, where emission is amplified between end facets.[20-23] Nevertheless, the efficiency of a Fabry–Pérot mode (FPM) is relatively low, because the reflection at the end facet is usually low for normal incidence at the interface between the gain material and air.[20,23] Another class of lasers utilizes whispering–gallery-type cavities in spherical and disk structures, where standing waves of circulating photonic modes are formed by multiple internal reflections along the cavity.[24-30] Since total internal reflection minimizes the mirror loss even without complex reflectors,[18,19] the whispering–gallery mode (WGM) proposes high efficiency of nanolasers for a broad range of applications.

Multicolor lasers can be attainable in heterostructure materials, where the band gap energies of individual composites determine the distinctive colors.[11-14] In alloyed systems of III–nitride (InGaN), electronic band structures are tunable to offer a wide range of colors from the ultraviolet to visible region, suggesting the potential heterostructure materials for efficient multicolor devices. However, multicolor lasers of heterostructures are mostly achieved using FPM,[11,14] despite the advantages of WGM.[24-30] Certainly, WGM in multiple-layered structures composed of III–nitride systems is expected to improve multicolor nanolasers. Furthermore, a deeper understanding of photonic modes in multiple-layered materials could inspire novel designs of switchable nanolasers, because FPM and WGM propagate in orthogonal directions.

In addition to waveguiding properties, light–matter interactions are enhanced in nanocavities, due to the comparable dimensions of materials to the wavelength of light, developing bosonic quasi-particles of exciton–polariton.[31-35] As composite particles of the strong coupling between confined photons and excitons, polaritons show the high propagation speed and low effective mass characteristic of their photonic nature as well as the nonlinearity

[a] Department of Chemistry, Kyung Hee University, Seoul 02447, Korea
E-mail: jaeksong@khu.ac.kr
[b] Department of Chemistry, Kookmin University, Seoul 02707, Korea
E-mail: yrdo@kookmin.ac.kr

†Electronic Supplementary Information (ESI) available: Experimental section, Exciton–polariton model, and Figs. S1-S15. See DOI: 10.1039/x0xx00000x

‡These authors contributed equally.

Published on 15 August 2025. Downloaded by Yunnan University on 8/23/2025 9:47:54 PM.

Nanoscale Accepted Manuscript

Please do not adjust margins

View Article Online
DOI: 10.1039/D5NR02460B

Published on 15 August 2025. Downloaded by Yunnan University on 8/23/2025 9:47:54 PM.

Nanoscale Accepted Manuscript

associated with their excitonic nature. Moreover, polaritons can occupy a single quantum state to form a coherent condensate, due to their bosonic nature. Although polaritons have been primarily investigated at a cryogenic temperature,[32] room-temperature polaritons have recently been observed in ZnO and GaN.[32,33] Besides, polariton lasers have been demonstrated at room temperature,[33,36] proposing potential platforms for quantum optical devices. Multicolor polariton lasers have also been developed in heterostructure nanomaterials,[36-38] where the evolution of polariton is supported by the non-classical and tunable effective indices in each layer. Accordingly, polaritonic devices are anticipated to serve as building blocks of future integrated circuits, although polariton lasers have been mostly considered for FPM. Since light–matter interactions are influenced by the shapes of nanostructures, the understanding of polaritonic WGM would improve the controllability and viability of optoelectronic devices.

In this work, we report tunable multicolor polariton nanolasers, which are achieved through the optical confinement effect and active waveguiding in disk-shaped heterostructures composed of III-nitride materials (GaN/InGaN/GaN). In the nanodisks, the characteristics of WGM indicate active waveguiding, while the formation of exciton–polariton facilitates polaritonic lasing of GaN at a low threshold. The polaritonic lasing of InGaN is also established in the heterostructure, although the small gain volume in the quantum well structure leads to weak amplification of lasing. Remarkably, the properties of InGaN lasing are distinct from those of GaN lasing, implying the unique polaritonic behavior of InGaN in the quantum well structure. Therefore, tunable dual-color polariton lasers are realized in disk-shaped heterostructures, where WGM enables the independent control of GaN and InGaN lasing.

2. Results and discussion

Whispering–Gallery Mode in Nanodisk Polariton Laser. Upon continuous excitation (325 nm, 10 W/cm^2) of disk-shaped GaN nanomaterials (Fig. S1) with a selectively fabricated length (~800 nm) and diameter (~1.4 μm) in an array (inset of Fig. 1a),[39,40] the photoluminescence shows the band edge emission (Fig. 1a), because the center wavelength of ~367 nm corresponds to the band gap energy of ~3.4 eV, as evidenced by absorption profiles (Fig. S2). An isolated disk (inset of Fig. 1a), which is separated from the array but retains a nearly unchanged length and diameter (Fig. S2), is also investigated using a microscope objective under ambient conditions (Fig. S3).[41,42] The luminescence wavelength of the isolated disk is analogous to that of the disks in the array (Fig. 1a), implying that the band edge emission is not affected by the separation processes. Notably, humps are observed in the luminescence spectrum of the single disk, which can be decomposed into a series of peaks. Since these humps are not found in the luminescence spectra of the disks in the array, the humps suggest the presence of cavity modes in the single disk, such as FPM and WGM (Fig. S4), where the emission is waveguided along the cavity.

With increase in pulsed excitation (355 nm), sharp peaks grow on the humps (Fig. 1b), supporting efficient waveguiding of a disk. The linewidth of a peak decreases to reach a quality factor ($\lambda/\Delta\lambda$) of ~1000 (Fig. S5), and the peak intensity increases superlinearly above the threshold (inset of Fig. 1b). The superlinearity is evidenced by the light-output/light-input relation ($I_{out} = a\, I_{in}^{s}$), where s is greater than 1 above the threshold (Fig. S5).[14,15] Therefore, the narrow linewidth and superlinear increase indicate stimulated emission in a single disk by active waveguiding and amplification within a cavity. It is noted that FPM of the laser is not highly favored due to the low reflection at the end facets for normal incidence. Even when polaritonic characteristics enhance the effective index and thus the reflection at the end facets,[20,23] the mirror loss still impedes the amplification of FPM, considering the small gain volume of the disk along the axial direction (~800 nm). In contrast, total internal reflection minimizes mirror loss to achieve efficient amplification of WGM,[24-30] as supported by the presence of strong rays in the tangential directions of the disk (Fig. 1c).[28-30] Besides, the spatial fringes, which are absent below the threshold (Fig. 1c), reveal the coherent nature of the lasing. With further increase in excitation, another hump evolves into a sharp peak with comparable linewidth and superlinearity (Fig. 1b), suggesting longitudinal modes due to the extended bandwidth range of optical gain at high carrier densities. Nevertheless, only a few lasing modes are observed in most disks, implying a narrow gain bandwidth mainly due to the small volume of the disks for optical amplification.

In general, the mode spacing of cavity modes (ΔE) depends on the cavity length (L) as described by the photonic model of $\Delta E = hc/nL$, where h is the Planck constant, c is the speed of light, and n is the refractive index.[14,20] For WGM in a disk with the diameter (D) of 1.4 μm ($L = 3nD$), however, the estimated spacing (~110 meV) deviates from the observed one (~15 meV), when the spacing is calculated using the normal refractive index (n = 2.6). Alternatively, the index is estimated to be ~20 based on the observed spacing. Indeed, the observed spacing does not agree with the estimated spacing of axial FPM (~300 meV) in a disk with a length (l) of 800 nm ($L = 2nl$) or radial FPM (~170 meV) in a disk with a diameter (D) of 1.4 μm ($L = 2nD$). In addition, the spacing is not uniform along the energy spectrum (Fig. 1b), indicating that the classical photonic model is not sufficient to describe lasing modes in a nanodisk.

When the wavelength of light is comparable to the dimension of a cavity, the confined photon strongly interacts with the exciton within the cavity. This light–matter interaction becomes even stronger with the enhancement of oscillator strength, which can be achievable through optical confinement effects in a nanocavity. Hence, the strong coupling between the confined photon and exciton develops a quasi-particle of exciton–polariton,[31-35] exhibiting distinct features compared to both photons and excitons. In particular, the dielectric function of the polariton is much influenced by its resonance with the exciton (see Electronic Supplementary Information for details),[31,32] leading to the distinguishable dispersion of polariton from the typical dispersion of photon (Fig. 1d). The characterizing features are derived from experimental observations (Fig. 1e) to describe the dispersion of polariton, because angle-resolved spectroscopy of the nanodisk is not effective with the current detection method. Since the effective index of the polariton

 This journal is © The Royal Society of Chemistry 20xx

View Article Online
DOI: 10.1039/D5NR02469B

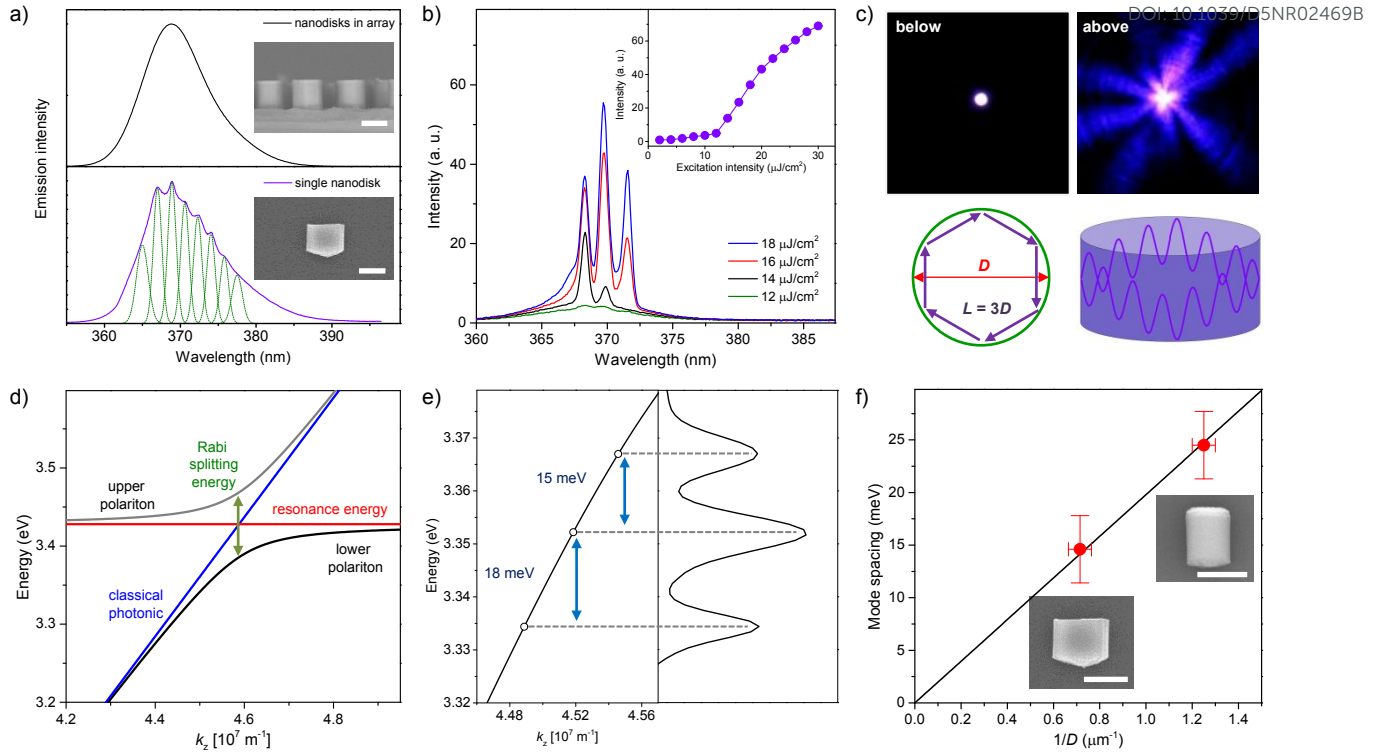

Fig. 1. (a) Photoluminescence spectra of GaN disks in the array (top) and a single disk (bottom). Insets show SEM images of nanodisks. Scale bars are 1 μm. (b) Lasing spectra of a single disk with increasing excitation intensity. Inset shows the emission intensities. (c) Optical images below and above the threshold with schematics of WGM in a disk. (d) The dispersion of polariton is compared to the classical dispersion of photon in a cavity. (e) The lasing spectrum (right) matches the energy–wavevector diagram of polariton near the resonance energy (left). (f) The observed mode spacing is compared to the simulated one as a function of the inverse diameter of disks. Insets show SEM images of nanodisks. Scale bars are 1 μm.

increases by up to 10-fold near the resonance regime (Fig. S6), the non-classical mode spacing is correlated to the energy-dependent dispersion in a lower branch of the polariton. Therefore, the unique spacing is ascribed to polaritonic dispersion, indicating the development of polariton in a nanodisk. The splitting energy is calculated to be ~0.12 eV (Fig. 1d), which is analogous to the Rabi energy in the strong coupling regime.[34,35]

The coherent eigenstates of polaritons can be formed through polariton–polariton scattering, leading to polaritonic lasing at a lower threshold than photonic lasing established by a population inversion.[32-35] Indeed, the lasing threshold is as low as 10 μJ/cm² (Fig. S6), although the thresholds of individual disks are not identical but mostly within the range of 10–20 μJ/cm², because the optical gain is influenced by various factors. At the threshold, the estimated carrier density is less than 5×10^{17} cm^{-3}, assuming that carriers are homogeneously distributed within a disk. This density is lower than the Mott density of GaN (~5.0×10^{18} cm^{-3}),[43,44] indicating that the exciton state remains stable even at the threshold, to facilitate the formation of exciton–polariton and thus polariton lasing. Yet, the spacing of WGM differs among individual disks (Fig. S6), because the light–matter interaction is affected by several features of disks, as the optical gain is, which alters the coupling strength (splitting energy) and thus strength-dependent dispersion of polariton. Moreover, slight variations in the disk diameters are responsible for the unequal spacing. Certainly, the mode spacing is inversely proportional to the diameter of the disks (Fig. 1f), supporting the presence of WGM with polaritonic characteristics (Fig. S7), rather than FPM along the axial direction. Consequently, the nonidentical spacing of WGM leads to indiscernible humps in the photoluminescence spectrum of the disks in the array (Fig. 1a), because the similar but unequal humps of individual nanodisks average out their contributions.

The peak positions of polaritonic lasing exhibit slight changes with carrier density, due to several factors.[31-35] With increasing carrier density, band-filling effects and multiparticle interactions can alter the peak positions. Besides, a decrease in exciton binding energy weakens the coupling strength of exciton–polariton. The effective index is also influenced by carrier density and temperature. Accordingly, the peak shift is attributed to the characteristics of exciton–polariton, which modify the coupling strength and effective index with carrier density.

Multicolor Whispering–Gallery Mode in Heterostructure Nanodisk Laser. The optical properties are further investigated in disk-shaped axial heterostructures,[39,40] which were prepared from an epitaxially-grown, sequentially-stacked wafer (Fig. S1). The alloy of In and Ga in

Published on 15 August 2025. Downloaded by Yunnan University on 8/23/2025 9:47:54 PM.

Nanoscale Accepted Manuscript

View Article Online
DOI: 10.1039/D5NR02469B

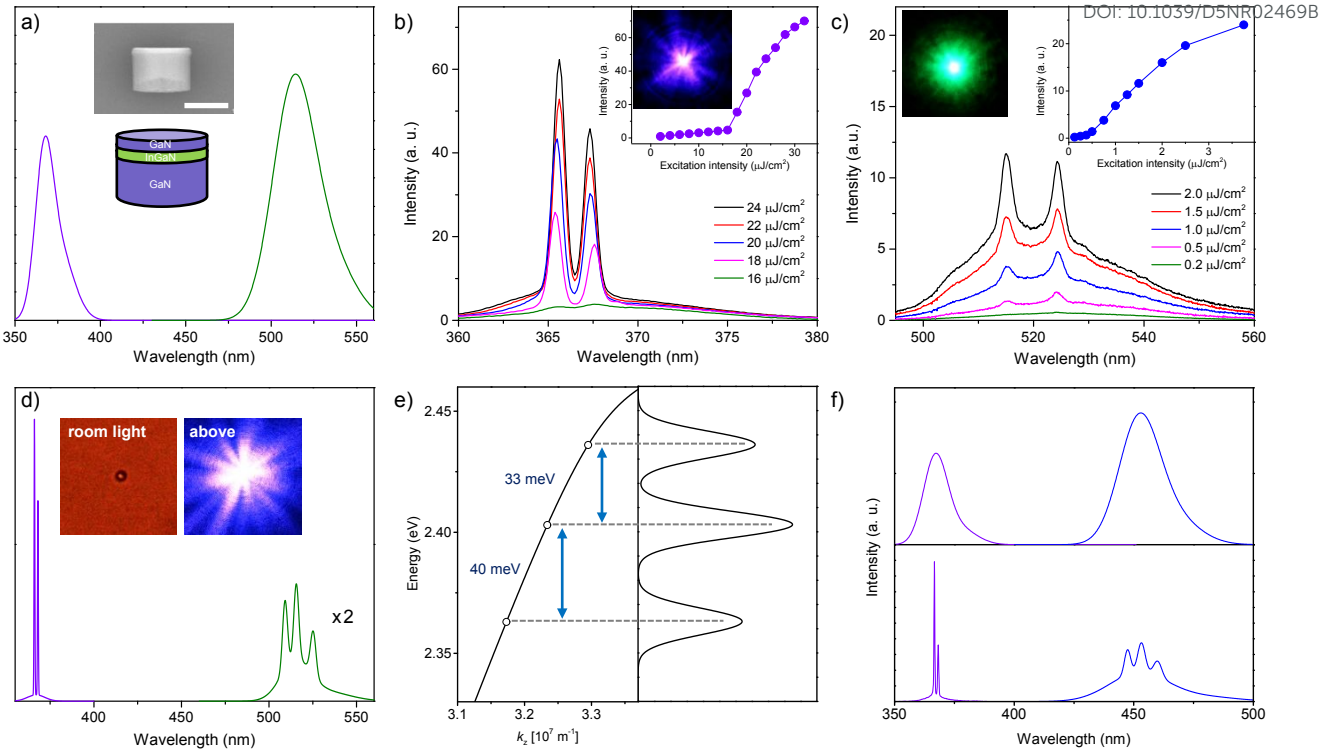

Fig. 2. (a) Photoluminescence spectrum of heterostructure nanodisk (GaN/InGaN-MQW/GaN). Insets show the SEM image and schematic view of heterostructure. Scale bar is 1 μm. (b) Lasing spectra in the luminescence region of GaN in a single heterostructure with increasing excitation intensity. Insets show the emission intensities and optical image above the threshold. (c) Lasing spectra in the luminescence region of InGaN in a single heterostructure. Insets show the emission intensities and optical image. (d) Lasing spectrum of a single disk. Insets show optical images under room light (left) and above the threshold (right). (e) The lasing spectrum of InGaN (right) matches the energy–wavevector diagram of polariton near the resonance energy (left). (f) Photoluminescence (top) and lasing (bottom) spectra of the heterostructure disk with MQW of $In_{0.2}Ga_{0.8}N$.

III-nitride system (InGaN) is employed for multiple quantum well (MQW) with multiple periods of InGaN/GaN to modulate the electronic band structures, GaN/InGaN-MQW/GaN (inset of Fig. 2a). The total length (~800 nm) and diameter (~1.4 μm) of the heterostructures remain unchanged from the homostructures, with the MQW thickness of ~100 nm (Fig. S2). Upon excitation of 325 nm, two emission bands are observed in the heterostructure (Fig. 2a), which are attributed to the emissions of GaN (~370 nm) and InGaN (~510 nm). The emission peak of GaN in the heterostructure is consistent with that in the homostructure, implying that In does not diffuse significantly into the GaN layers during the synthesis process. The emission in the visible region indicates the band edge transition of InGaN ($In_{0.3}Ga_{0.7}N$) with a band gap energy of ~2.45 eV,[12,15] as evidenced by absorption profiles (Fig. S2). Hence, the optical features demonstrate the successful fabrication of heterostructures with well-defined MQW. Remarkably, the high intensity of the InGaN emission (>60%), compared to its volume ratio (<10%), suggests that the emission rate of InGaN is enhanced in MQW structures and the carriers in the GaN layers transfer to InGaN along the band potentials in the heterostructure nanodisks (Fig. S8).

With an increase in pulsed excitation, sharp peaks are observed in both GaN and InGaN emissions, suggesting efficient waveguiding and amplification in the heterostructure nanodisk. In the luminescence region of GaN (Fig. 2b), the linewidth and superlinearity of the sharp peaks in the heterostructure are similar to those in the homostructure, indicating the evolution of WGM, as supported by the strong directional rays in the disk (inset of Fig. 2b). The peak positions also change slightly with excitation intensity, due to the altered characteristics of exciton–polariton with carrier density. The lasing threshold in the heterostructure is not much different from that in the homostructure (Fig. S8). In fact, GaN emission is reabsorbed by InGaN during roundtrips for FPM in the axial heterostructure, which is typically responsible for an elevated threshold.[14,36] However, WGM, which propagates perpendicular to the axial direction, avoids the reabsorption of GaN emission by InGaN, leading to the comparable threshold to the homostructure. Nevertheless, the gain volume of the GaN layers is reduced by substitution with InGaN. Moreover, carriers in the GaN layers transfer to InGaN, although carriers in GaN layers distant from InGaN layers do not completely transfer, as evidenced by the nontrivial emission of GaN (Fig. 2a). Accordingly, the comparable threshold between the homostructure and heterostructure further suggests relatively localized amplification for WGM lasing (Fig. S8), which minimizes the influence of the reduced volume and carrier transfer.

Published on 15 August 2025. Downloaded by Yunnan University on 8/23/2025 9:47:54 PM.

Nanoscale Accepted Manuscript

This journal is © The Royal Society of Chemistry 20xx

Please do not adjust margins

View Article Online
DOI: 10.1039/D5NR02460B

Published on 15 August 2025. Downloaded by Yunnan University on 8/23/2025 9:47:54 PM.

The similar mode spacing between the homostructure and heterostructure is another evidence for polaritonic WGM (Fig. S8), because the stable exciton state is expected at the threshold in the heterostructure to develop exciton–polariton and thus polariton lasing. In FPM, GaN polariton propagates in InGaN layers, where the effective index is reduced by the energy-dependent dispersion of polariton (Fig. S9), leading to the different spacing from the homostructure.[37,38] In WGM, however, GaN polariton does not propagate in InGaN layers during roundtrips, showing the analogous spacing of polaritonic WGM to the homostructure.

In the luminescence region of InGaN, narrow peaks are also found (Fig. 2c), while the formation of WGM is supported by the inversely proportional spacing to the diameter of the heterostructure (Fig. S10) and the directional rays with spatial fringes (inset of Fig. 2c). Remarkably, the threshold of InGaN is much lower than that of GaN, which is ascribable to the enhanced emission rate and carrier transfer from GaN,[12-14] as demonstrated by the high emission intensity compared to the volume ratio. Nevertheless, the linewidth and superlinearity of InGaN lasing are inferior to those of GaN lasing (inset of Fig. 2c). Indeed, strong amplification processes are hindered by the easy saturation of the small gain volume in the MQW structure of InGaN (Fig. S11), although the gain process is facilitated at low excitation intensity by the enhanced emission rate, carrier transfer, and waveguiding with total internal reflection.

The mode spacing is also different between GaN and InGaN (Fig. 2d), despite the formation of WGM in the same disk. Certainly, the stable exciton state of InGaN is expected, because the carrier density would be ~1.1×10^{16} cm^{-3} at the threshold (~0.5 μJ/cm^2). Even when the carrier transfer from GaN is considered, the carrier density of InGaN ($< 2.0 \times 10^{17}$ cm^{-3}) is lower than the Mott density. Hence, InGaN polariton is developed to enhance the effective index in the InGaN layers (Fig. S9), as GaN polariton is in the GaN layers. However, the polariton might not be completely confined in each InGaN layer (<10 nm) of the MQW structure. In other words, the InGaN polariton also propagates in the neighboring GaN layers, where the effective index of the polariton is not much enhanced due to the energy-dependent dispersion of the polariton. Indeed, the observed spacing (ΔE = 33 meV) is larger than the expected spacing of the polariton model (ΔE = ~15 meV). Yet, the observed spacing is still smaller than the expected spacing of the classical model (ΔE = ~110 meV), implying that the polaritonic effect works in InGaN. Accordingly, the unusual spacing is associated to the polaritonic dispersion near the resonance regime (Fig. 2e), although the loosely confined polariton in the MQW structure leads to unique features. When the coupling energy is estimated from the observed spacing (Fig. S11), the coupling strength of InGaN is reduced to demonstrate the influence of the loose confinement. Therefore, the lasing properties, such as the threshold, superlinearity, and spacing, are different between GaN and InGaN, despite the formation of WGM in the same disk.

The polariton in the MQW structure is further investigated in another system of InGaN, whose color is tuned by the ratio of In from green (~510 nm) of $In_{0.3}Ga_{0.7}N$ to blue (~450 nm) of $In_{0.2}Ga_{0.8}N$. The total length and diameter of the heterostructures remain unchanged with the similar thickness of MQW. The high intensity of the InGaN emission (Fig. 2f), compared to the volume ratio, supports the enhanced emission rate in the MQW structure and carrier transfer from GaN, representing the successful fabrication of the heterostructures. The InGaN lasing is also found with the spatial fringes of emission at a low threshold, although the linewidth and superlinearity indicate weak amplification due to the small gain volume (Fig. S12). The mode spacing is analogous in the two types of heterostructures (Fig. S12), confirming that the unusual spacing is attributable to the dispersion of the loosely confined polariton. Consequently, polariton lasing is tunable in the visible region using alloyed systems in the heterostructure, where the lasing of GaN and InGaN could be independently controlled using the characteristics of the polariton and WGM.

Transverse Mode of Whispering–Gallery Mode in Nanodisk. In the WGM of disk-shaped waveguides, a few transverse modes, such as transverse magnetic (TM) and transverse electric (TE) modes, can develop. In general, the lasing threshold of TM modes is lower than that of TE modes, because the effective indices of TM modes are larger to induce a higher gain.[25,27] Hence, the features of transverse modes are investigated using polarization-dependent intensities in a homostructure (Fig. S13),[45,46] because TM and TE modes are distinguishable by their orthogonal field distributions. Certainly, the measured intensities indicate the anisotropic polarization of lasing (Fig. 3a), indicating the development of the fundamental (TM) mode. In addition, lasing peaks with unusual spacing exhibit a similar degree of polarization (Fig. S13), which confirms that the two peaks belong to the fundamental mode. Accordingly, polaritonic effects are further supported by the unique spacing of the two peaks with comparable polarization, excluding the possibility that the non-classical spacing is correlated to the simultaneous evolution of two types of transverse modes. Likewise, the simultaneous development of fundamental and high-order modes can be ruled out by the similar degree of polarization observed in lasing peaks with unusual spacing.

Analogous degree of polarization is also observed in the lasing peaks (**A** and **B**) of a heterostructure (Fig. 3b), confirming the development of TM modes. Remarkably, the lasing peak with distinct polarization is often found in both the homostructure and heterostructure (Fig. 3c), despite the reduced intensity, when the optical gain is high enough to sustain two types of transverse modes. The minor peak (**α**) is attributed to the TE mode, while the major peak (**β**) is the TM mode with a higher gain, because the polarization dependence shows the orthogonal field distributions.[45,46] The lasing of InGaN in a heterostructure also exhibits comparable polarization between lasing peaks with non-classical spacing (**a** and **b**), indicating that the two peaks belong to the fundamental mode, to support the effects of polaritonic dispersion (Fig. 3d). However, the degree of polarization is different between the lasing of InGaN and GaN (Fig. S13), despite the fundamental transverse mode in the equivalent resonator. Since the degree of polarization depends on the degree of amplification,[25,27] the low degree of polarization is ascribed to reduced amplification by the saturation of the gain in the thin layers of the MQW structure, as are the superlinearity and quality factor of InGaN.

Nanoscale Accepted Manuscript

Please do not adjust margins

View Article Online
DOI: 10.1039/D5NR02469B

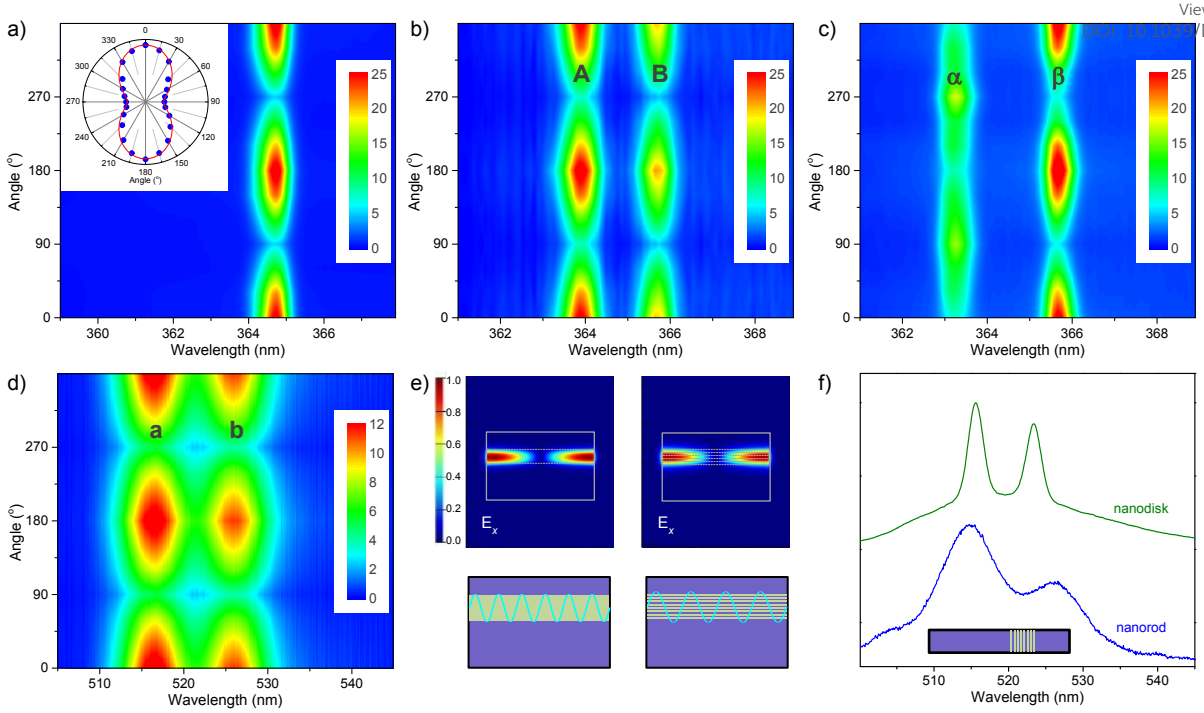

Fig. 3. (a) Lasing spectra of GaN in a homostructure are plotted along the polarization angle. The polarization angle for TM modes is denoted as 0°. Inset shows the polar plot of lasing intensities. (b) Lasing spectra of GaN in a heterostructure with a similar degree of polarization in peaks **A** and **B**. (c) Lasing spectra of GaN with distinct polarization in peaks **α** and **β**. (d) Lasing spectra of InGaN with comparable polarization in peaks **a** and **b**. (e) Simulated electric field distributions of fundamental modes in axial heterostructures with a single quantum well (left) and multiple quantum wells (right). (f) A lasing spectrum of InGaN in a nanorod is compared to that in a nanodisk.

Whispering–Gallery Mode in Multiple Quantum Well of Heterostructure Nanodisk. To understand WGM of MQW structures in more detail, the electric field distributions of InGaN are calculated using a finite-difference eigenmode simulation (MODE solutions, Lumerical Inc.).[14,15] In an axial heterostructure, the electric field of the fundamental mode is distributed along the MQW structure due to the thin layers of InGaN (Fig. 3e),[47-49] supporting the loosely confined polariton model. Notably, these distributions could work differently in a rod-shaped axial heterostructure (Fig. S14), which is more suitable for the development of FPM. Accordingly, the optical features are investigated in the heterostructure nanorod with a comparable cavity length. In InGaN lasing, the linewidth is broader (Fig. 3f) and the threshold is higher (Fig. S15) in the nanorod than in the nanodisk, although the observed modes in both the nanorod and nanodisk would be the fundamental mode of the lowest threshold. Certainly, the optical gain of FPM is not high, because the low reflection at the end facets for normal incidence inevitably induces mirror loss. Besides, emission is amplified only in the thin InGaN layers during roundtrips for FPM, whereas emission is fully amplified along the roundtrips for WGM. Hence, the optical gain of WGM is improved in the MQW structure, leading to a narrower linewidth and lower threshold than FPM. The spacing of FPM is also distinct from that of WGM (Fig. 3f), even in the comparable cavity length, although the spacing of FPM (ΔE = ~80 meV) deviates from the classical model to evidence the polaritonic effect. During roundtrips for FPM along the nanorod, the InGaN polariton experiences the enhanced index only in the thin InGaN layers (Fig. S14), whereas the polariton mostly propagates in the GaN layers of near-normal index (Fig. S9). Therefore, the optical gain and spacing of InGaN are different between WGM and FPM, demonstrating the superior features of WGM over FPM.

Overall, the optical properties indicate the development of polaritonic WGM in a nanodisk. First, the non-classical spacing of lasing is attributed to polaritonic dispersion near the resonance regime (Fig. 4a), despite slight variance in individual nanodisks due to the energy-dependent and strength-dependent dispersion of polariton. Second, the mode spacing is inversely proportional to the diameter (Fig. 4b), supporting polaritonic WGM. Third, the mode spacing is different between GaN and InGaN in an equivalent cavity (Fig. 4c), due to the confinement effects in the MQW structure. Fourth, the unusual spacing of InGaN is ascribed to the reduced coupling energy of loosely confined polariton in the MQW structure (Fig. 4d). Fifth, the mode spacing of InGaN is independent of band gap energies (Fig. 4e), because polaritonic dispersion near the resonance energy is primarily responsible for the unique spacing. Sixth, the spacing of FPM is different from that of WGM (Fig. 4f), despite a comparable cavity length, because the effective index in each layer is influenced by the resonance energy of the composite materials.

Published on 15 August 2025. Downloaded by Yunnan University on 8/23/2025 9:47:54 PM.

Nanoscale Accepted Manuscript

This journal is © The Royal Society of Chemistry 20xx

View Article Online
DOI: 10.1039/D5NR02469B

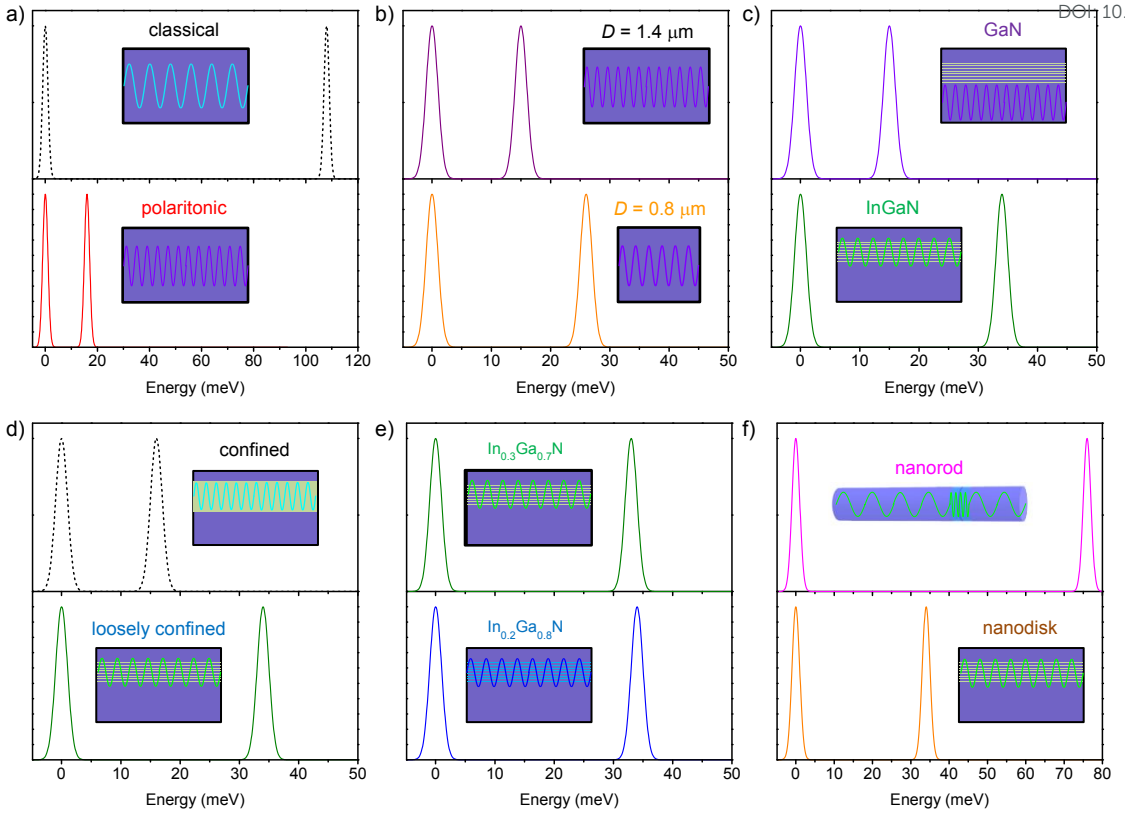

Fig. 4. (a) The mode spacing of GaN lasing estimated by the classical model is compared to the observed spacing to support the polaritonic model in nanodisks. (b) The mode spacing of GaN lasing in nanodisks of different diameters. (c) The mode spacing of GaN and InGaN lasing in the same nanodisk. (d) The mode spacing of InGaN lasing estimated by the polaritonic model is compared to the observed spacing to indicate the effect of loose confinement. (e) The mode spacing of InGaN lasing in two alloyed systems. (f) The mode spacing of InGaN lasing in a heterostructure nanorod is compared to that in a heterostructure nanodisk with a comparable cavity length.

3. Conclusions

We realize tunable dual-color nanolasers using disk-shaped axial heterostructures for the first time, where WGM affords independent control of GaN and InGaN lasing. The nanodisks fabricated in an array are individually separated and selectively investigated. With increasing intensity, the humps in the band edge emission become narrowed with a superlinear increase, indicating stimulated emission by active waveguiding in the nanodisks. The spatial fringes of directional rays confirm the coherent nature of lasing aided by total internal reflection. The observed features suggest that optical confinement effects develop exciton–polariton with unique dispersion, while efficient waveguiding leads to polaritonic lasing of GaN. The lasing of InGaN is different from that of GaN, despite stimulated emission occurring in the same resonator, due to the small gain volume and loosely confined polariton of InGaN. The alloyed systems of InGaN provide tunable laser color in the visible region, while the dual colors of GaN and InGaN are independently controllable in a single nanodisk. Therefore, polaritonic WGM is beneficial to the evolution of multicolor lasers, proposing the potential for next-generation nanophotonic devices using band gap tuning, optical confinement effect, and active waveguiding.

4. Experimental section

Since the fabrication procedures of nanodisks using the top–down approach have been described elsewhere,[39,40] a few essentials specific to the present work are outlined here (see Electronic Supplementary Information for details). Homostructure nanodisks were fabricated using an epitaxially-grown wafer of GaN (Fig. S1). A preformed pattern was transferred to prepare a disk array *via* wet and dry etching (Fig. S2). The etching and sonication were performed to separate the disks from the wafer, after which they were purified and stored in an acetone solution. Heterostructure nanodisks were prepared using an epitaxially-grown, sequentially-stacked wafer, consisting of GaN, MQW of InGaN/GaN, and GaN layers, GaN/InGaN-MQW/GaN. In the MQW structure, multiple periods of InGaN/GaN were stacked. After the preformed pattern was transferred *via* wet and dry etching, the heterostructure disks were separated from the wafer. Two types of heterostructures were prepared with controlled ratio of In for the nominal composition of $In_{0.2}Ga_{0.8}N$ and $In_{0.3}Ga_{0.7}N$. The separated disks were transferred onto a fused silica substrate to examine their optical properties under ambient conditions.[41,42] An individual disk was selectively investigated through a microscope objective by either the continuous wave of a He–Cd laser (325 nm)

Published on 15 August 2025. Downloaded by Yunnan University on 8/23/2025 9:47:54 PM.

Nanoscale Accepted Manuscript

View Article Online
DOI: 10.1039/D5NR02459B

or the pulses of a Ti:sapphire laser (355 nm). The excitation diameter at the substrate was ~30 μm to ensure homogeneous excitation (Fig. S3). The emission collected using the same objective was resolved using a monochromator and detected using a photomultiplier. For polarization-dependent measurements, the emission was further filtered through a polarizer.

Conflicts of interest

There are no conflicts to declare.

Data availability

All data generated or analyzed during this study are included in this published article and its ESI.†

Acknowledgements

This work was supported by the National Research Foundation of Korea (NRF) grant funded by the Korea government (RS-2024-00336065 and 2021R1A2C2009521).

References

1. J. J. Wierer Jr, A. David and M. M. Megens, *Nat. Photonics*, 2009, **3**, 163-169.

2. V. K. Sharma, S. T. Tan, Z. Haiyang, S. Shendre, A. Baum, F. Chalvet, J. Tirén and H. V. Demir, *Adv. Opt. Mater.*, 2021, **9**, 2100072.

3. V. K. Sharma and H. V. Demir, *ACS Photonics*, 2022, **9**, 1513-1521.

4. A. Karami, T. J. de Prinse, N. A. Spooner, S. P. Kidd, C. J. Sumby and J. Bi, *ACS Appl. Nano Mater.*, 2023, **6**, 7031-7043.

5. Q. Zhou, B. M. Wirtz, T. H. Schloemer, M. C. Burroughs, M. Hu, P. Narayanan, J. Lyu, A. O. Gallegos, C. Layton, D. J. Mai and D. N. Congreve, *Adv. Mater.*, 2023, **35**, 2301563.

6. S. Deshpande, J. Heo, A. Das and P. Bhattacharya, *Nat. Commun.*, 2013, **4**, 1675.

7. J. Shi, J. Zhang, L. Yang, M. Qu, D.-C. Qi and K. H. L. Zhang, *Adv. Mater.* **2021**, *33*, 2006230.

8. J.-E. Ryu, S. Park, Y. Park, S.-W. Ryu, K. Hwang and H. W. Jang, *Adv. Mater.*, 2023, **35**, 2204947.

9. Y. Luo, D. Wang, Y. Kang, S. Fang, X. Liu, W. Chen, H. Yu, H. Jia, M. H. Memon, H. Zhang, D. Luo, X. Sun, L. Li, J.-H. He and H. Sun, *Adv. Opt. Mater.*, 2023, **11**, 2300129.

10. S. Sarker, Y. Wang, C. Benyacko, Y. Guan, S. Yoshida, H. Yennawar, J. He, Z. Mao and V. Gopalan, *Adv. Opt. Mater.*, 2024, **12**, 2401437.

11. F. Qian, Y. Li, S. Gradečak, H.-G. Park, Y. Dong, Y. Ding, Z. L. Wang and C. M. Lieber, *Nat. Mater.*, 2008, **7**, 701-706.

12. X. Zhou, M.-Y. Lu, Y.-J. Lu, E. J. Jones, S. Gwo and S. Gradečak, *ACS Nano*, 2015, **9**, 2868-2875.

13. H. K. Park, S. W. Yoon, Y. J. Eo, W. W. Chung, G. Y. Yoo, J. H. Oh, K. N. Lee, W. Kim and Y. R. Do, *Sci. Rep.*, 2016, **6**, 28312.

14. H. Zong, Y. Yang, C. Ma, X. Feng, T. Wei, W. Yang, J. Li, J. Li, L. You, J. Zhang, M. Li, C. Pan, X. Hu and B. Shen, *ACS Nano*, 2017, **11**, 5808-5814.

15. C. Li, J. B. Wright, S. Liu, P. Lu, J. J. Figiel, B. Leung, W. W. Chow, I. Brener, D. D. Koleske, T.-S. Luk, D. F. Feezell, S. R. J. Brueck and G. T. Wang, *Nano Lett.*, 2017, **17**, 1049-1055.

16. T. Feng, S. Zhang, K. Yang, Q. Chen, M. Liang, J. Yan, X. Yi, J. Wang, J. Li and Z. Liu, *Adv. Opt. Mater.*, 2022, **10**, 2201262.

17. B. Park, J. K. Lee, C. T. Koch, M. Wölz, L. Geelhaar and S. H. Oh, *Adv. Sci.*, 2022, **9**, 2200323.

18. C.-F. Lai, J.-Y. Chi, H.-H. Yen, H.-C. Kuo, C.-H. Chao, H.-T. Hsueh, J.-F. T. Wang, C.-Y. Huang and W.-Y. Yeh, *Appl. Phys. Lett.*, 2008, **92**, 243118.

19. J. B. Wright, S. Liu, G. T. Wang, Q. Li, A. Benz, D. D. Koleske, P. Lu, H. Xu, L. Lester, T. S. Luk, I. Brener and G. Subramania, *Sci. Rep.*, 2013, **3**, 2982.

20. J. C. Johnson, H. Yan, P. Yang and R. J. Saykally, *J. Phys. Chem. B*, 2003, **107**, 8816-8828.

21. Y. Fu, H. Zhu, C. C. Stoumpos, Q. Ding, J. Wang, M. G. Kanatzidis, X. Zhu and S. Jin, *ACS Nano*, 2016, **10**, 7963-7972.

22. C. Li, S. Liu, T. S. Luk, J. J. Figiel, I. Brener, S. R. J. Brueck and G. T. Wang, *Nanoscale*, 2016, **8**, 5682.

23. M. Behzadirad, M. Nami, N. Wostbrock, M. R. Z. Kouhpanji, D. F. Feezell, S. R. J. Brueck and T. Busani, *ACS Nano*, 2018, **12**, 2372-2380.

24. L. Ma, H. Zhong, T. Yang, L. Ying, J. Chen, Z. Su, S. Chen, G. Weng, Y. Mei and B. Zhang, *Laser Photon. Rev.*, 2025, **19**, 2500151.

25. Q. Zhang, S. T. Ha, X. Liu, T. C. Sum and Q. Xiong, *Nano Lett.*, 2014, **14**, 5995-6001.

26. S. Yakunin, L. Protesescu, F. Krieg, M. I. Bodnarchuk, G. Nedelcu, M. Humer, G. D. Luca, M. Fiebig, W. Heiss and M. V. Kovalenko, *Nat. Commun.*, 2015, **6**, 8056.

27. Q. Liao, K. Hu, H. Zhang, X. Wang, J. Yao and H. Fu, *Adv. Mater.*, 2015, **27**, 3405-3410.

28. S. Chen, X.-D. Wang, M.-P. Zhuo, G.-Q. Wei, J.-J. Wu and L.-S. Liao, *Adv. Opt. Mater.*, 2022, **10**, 2101931.

29. S. J. Neuhaus, E. Marino, C. B. Murray and C. R. Kagan, *Nano Lett.*, 2023, **23**, 645-651.

30. Z.-H. Lin, S. Kushida, F.-C. Lin, J.-Y. Chen, A. K. Singh, Y. Yamamoto and J.-S. Huang, *Nano Lett.*, 2023, **23**, 6512-6519.

31. L. K. van Vugt, B. Piccione, C.-H. Cho, P. Nukala and R. Agarwal, *Proc. Natl. Acad. Sci. U. S. A.*, 2011, **108**, 10050-10055.

32. A. Das, J. Heo, M. Jankowski, W. Guo, L. Zhang, H. Deng and P. Bhattacharya, *Phys. Rev. Lett.*, 2011, **107**, 066405.

33. D. Vanmaekelbergh and L. K. van Vugt, *Nanoscale*, 2011, **3**, 2783.

34. T. J. S. Evans, A. Schlaus, Y. Fu, X. Zhong, T. L. Atallah, M. S. Spencer, L. E. Brus, S. Jin and X.-Y. Zhu, *Adv. Opt. Mater.*, 2018, **6**, 1700982.

35. M. Liu, M. Jiang, Q. Zhao, K. Tang, S. Sha, B. Li, C. Kan and D. N. Shi, *ACS Appl. Mater. Interfaces*, 2023, **15**, 13258-13269.

36. S. Y. Chun, G. Y. Yoo, S. Jeong, S. M. Park, Y. J. Eo, W. Kim, Y. R. Do and J. K. Song, *Nanoscale*, 2019, **11**, 14186.

37. S. J. Won, M. Ko, H. S. Shim, S. Lee, S. Nam, H. J. Kim, S. Yun, S. M. Park, Y. R. Do and J. K. Song, *ACS Photonics*, 2022, **9**, 3234-3244.

Published on 15 August 2025. Downloaded by Yunnan University on 8/23/2025 9:47:54 PM.

Nanoscale Accepted Manuscript

This journal is © The Royal Society of Chemistry 20xx

Please do not adjust margins

Please do not adjust margins

View Article Online
DOI: 10.1039/D5NR02469B

38. S. Nam, S. Lee, S. Jeong, M. Ko, H. S. Shim, E. Hong, S. M. Park, Y. R. Do and J. K. Song, *Adv. Opt. Mater.*, 2024, **12**, 2301213.

39. M. Ko, E. Hong, Y. J. Eo, S. Lee, S. Kim, H. J. Kim, K. N. Lee, C. Kim and Y. R. Do, *Adv. Funct. Mater.*, 2024, **34**, 2303727.

40. M. Ko, S. Kim, Y. Jeong, Y. Oh, S. Jeong, K. N. Lee, Y. Park, J. K. Song and Y. R. Do, *Appl. Surf. Sci.*, 2025, **681**, 161446.

41. N. S. Han, H. S. Shim, S. Lee, S. M. Park, M. Y. Choi and J. K. Song, *Phys. Chem. Chem. Phys.*, 2012, **14**, 10556-10563.

42. K. Park, J. W. Lee, J. D. Kim, N. S. Han, D. M. Jang, S. Jeong, J. Park and J. K. Song, *J. Phys. Chem. Lett.*, 2016, **7**, 3703-3710.

43. J. C. Johnson, H.-J. Choi, K. P. Knutsen, R. D. Schaller, P. Yang and R. J. Saykally, *Nat. Mater.*, 2002, **1**, 106.

44. J. Heo, S. Jahangir, B. Xiao and P. Bhattacharya, *Nano Lett.*, 2013, **13**, 2376-2380.

45. H. Baek, J. K. Hyun, K. Chung, H. Oh and G.-C. Yi, *Appl. Phys. Lett.*, 2014, **105**, 201108.

46. X. Liu, S. T. Ha, Q. Zhang, M. de la Mata, C. Magen, J. Arbiol, T. C. Sum and Q. Xiong, *ACS Nano*, 2015, **9**, 687-695.

47. J. T. Robinson, K. Preston, O. Painter and M. Lipson, *Opt. Express*, 2008, **16**, 16659-16669.

48. Y.-D. Yang, M. Tang, F.-L. Wang, Z.-X. Xiao, J.-L. Xiao and Y.-Z. Huang, *Photonics Res.*, 2019, **7**, 594-607.

49. G. Zhu, J. Li, N. Zhang, X. Li, J. Dai, Q. Cui, Q. Song, C. Xu and Y. Wang, *Sci. Rep.*, 2020, **10**, 253.

Published on 15 August 2025. Downloaded by Yunnan University on 8/23/2025 9:47:54 PM.

Nanoscale Accepted Manuscript

Please do not adjust margins

View Article Online
DOI: 10.1039/D5NR02469B

All data generated or analyzed during this study are included in this published article and its ESI.

Published on 15 August 2025. Downloaded by Yunnan University on 8/23/2025 9:47:54 PM.

Nanoscale Accepted Manuscript